CONF-9308130--9

WSRC-MS-92-366

MEASUREMENT OF LOCAL VOID FRACTION IN A RIBBED ANNULUS (U)

by J. L. Steimke

Westinghouse Savannah River Company
Savannah River Site
Aiken, South Carolina 29808

Other Authors:

A paper proposed for Presentation/Publication
at/in the National Heat Transfer Conference
Atlanta, GA
08/08-11/93

DISCLAIMER

WSRC-MS-92-366 December 22, 1992

Measurement of Local Void Fraction in a Ribbed Annulus

Background

The computer code FLOWTRAN-TF is used to analyze hypothetical hydraulic accidents for K Reactor, a nuclear production reactor at the Savannah River Site. During a hypothetical Large Break Loss-of-Coolant Accident (LOCA), reactor assemblies would contain a two-phase mixture of air and water which flows downward. Reactor assemblies consist of nested, ribbed annuli. Longitudinal ribs divide each annulus into four subchannels. For accident conditions, air and water can flow past ribs from one subchannel to another. For FLOWTRAN-TF to compute the size of those flows, it is necessary to know the local void fraction in the region of the rib. Measurements have previously been made of length-average void fraction in a ribbed annulus by Whatley [1] and Flach [2]; however, no direct measurements were available of local void fraction. A literature survey revealed no local void fraction data for the conditions of interest. Due to the lack of data, a test was designed to measure local void fraction at the rib. One question addressed by the test was whether void fraction at the rib is solely a function of azimuthal-average void fraction or a function of additional variables such as pressure boundary conditions.

Summary

Various air-water downward flows were established in a vertical ribbed annulus 4.0 m long. The flow regime was usually slug or churn. The inlet pressure was always atmospheric. Two different pressure boundary conditions were applied at the bottom of the annulus. Length-average void fractions were measured using quick-closing bladder valves and were plotted in drift flux form. An analysis was used to relate the length-average void fraction to the azimuthal-average void fraction at the elevation of the densitometer measurement. The two void fractions could be different if void fraction varied with elevation. However, the two void fractions were found to be nearly equal (±0.03). A gamma densitometer was used to measure local void fractions inside the annulus at the rib. The sampling volume for the gamma densitometer was a cylinder with diameter of 11 mm, centered on two opposite ribs and located 1.5 m below the top bladder valve. The local void fraction at the rib was 44% of the azimuthal-average void fraction at the elevation of the measurement. Changing the bottom pressure boundary condition made no significant change in this relationship; therefore, the data support the hypothesis that void fraction at the rib is solely a function of azimuthal-average void fraction. For some runs the

densitometer beam was moved to other azimuthal positions in increments of 15° measured from the rib. For those positions the local void fraction was nearly uniform, larger than the local void fraction at the rib and about the same as the length-average void fraction.

Literature Survey

The spatial variations in local void fraction reported here have been referred to as lateral phase distribution phenomena. Lahey [3] gives a good survey of the subject. Oshinowa and Charles [4] photographed air-water upward and downward flows in a 25.4 mm diameter transparent pipe and found that the void fraction was higher in the middle of the pipe than at the walls, a phenomenon they called "void coring." Herringe and Davis [5] used an electrical resistivity probe to measure local void fractions for upward flow in a 51.6 mm pipe and found that the void profile peaked near the wall in some cases. Valukina et al. [6] generated monodisperse air bubbles and injected them into an upward water flow in a pipe, using electrical resistance probes to measure local void fraction. They found peaks in the void fraction distribution near the wall. Zun [7] used a laser to count air bubbles in a co-current upward flow and found a peak in the void fraction distribution near the wall. Nakoryakov et al. [8], measured the local void fraction for upflow in an 86 mm pipe using the same method as Herringe and Davis. For low gas flow to liquid flow ratios the void peaked near the wall and for high gas flow to liquid flow ratios the void peaked at the centerline. Sadatomi and Sato [9] measured both local and average void fractions and pressure drops for air-water upward flows through four types of flow channels: circular, annulus, rectangular and isosceles triangular. A needle contact probe was used to map the distribution of void fraction in the flow channels. For all shapes of flow channels the void fraction was least near the walls. Gorelik et al. [10] and Wang et al. [11] measured local void fractions with a hot film probe for both upward and downward air-water flows in a circular tube. They observed void coring for downward flows. For upward flow the maximum void fraction was located close to the wall. Bentley and Ruggles [12] measured the local void fraction in a rectangular vertical channel using the absorption of visible light by ink-dyed water that flowed along with air up the channel. The pattern of light passing through the channel was imaged by a video camera, and a calibration curve was used to convert gray scales to local void fractions. Only spatially averaged data were presented.

Present Test Apparatus

The present test apparatus consisted of a ribbed annulus Whatley [1], a 1.8-m long inlet section above it to develop the two-phase flow; an outlet section which controls the outlet pressure by means of a liquid level; a gamma densitometer; instrumentation to measure water

and air flow, pressure, temperature; and a data acquisition system. The inner and outer diameters of the annulus were 94 and 102 mm. The hydraulic diameter was 7.4 mm and the flow area was 1190 mm^2. Each rib was 1.5 mm wide and 3.4 mm tall. The ribbed annulus contained two specially designed bladder valves that acted as quick closing valves to measure overall void fraction. The bottom of the top valve was 200 mm below the top of the annulus and the top of the bottom valve was 150 mm above the bottom of the annulus. Normally the rubber bladders sat in recesses within the wall of the inner surface of the annulus such that the surface of the annulus was smooth. The ribs were removed in the vicinity of the bladder valves. There were also pressure taps at six axial locations on the annulus.

The principle of operation of the gamma densitometer is that a gamma beam passing through an air-water mixture is attenuated in proportion to the mass it encounters. Therefore, the greater the void fraction, the less the mass in the beam and the larger the number of gamma photons that pass through to a detector. The gamma densitometer consisted of a shielded cask containing a cesium-137 gamma source, a pneumatic controller for the gamma source, three gamma radiation detectors, three high-voltage power supplies and three signal amplifiers. Air pressure applied remotely was used to shift the source capsule in front of the cask's collimator, a block of tungsten with three horizontal holes drilled through it at different angles. For these tests, only the middle collimator hole and the corresponding detector were used.

The gamma densitometer source cask and detectors were fastened to a base and positioned so that the gamma beam crossed the ribbed annulus 1.52 m below the top bladder valve. For most tests the beam was centered on two opposite ribs, as shown in Figure 2. For a few tests the assemblage was rotated around the axis of the annulus so that the local void fraction was measured at different azimuthal locations. The gamma densitometer always measured the arithmetic average of the local void fractions at two regions 180° apart on the annulus. However, because of symmetry the time averages of those two void fractions were expected to be the same. Angular alignment was facilitated by marks inked on the base of the gamma densitometer and also on the outside of the annulus. The accuracy of the angular placement was ± 3°.

The gamma detector signal was noisy because the detector responds to individual photons. Therefore the output of the detector was passed through a 60 Hz low pass filter and recorded every 50 ms on a data acquisition system for about a minute. The signals from water and air flowmeters and pressure gages were also recorded.

Test Procedure

Two shakedown tests were run with the gamma densitometer [13]. The first determined the effective diameter of the gamma beam. The diameter of each of the three holes in the tungsten collimator was 6.4 mm. However, the beam diameter might have been larger due to

spreading. The power profile of the gamma beam was measured by traversing a 76 mm thick block of aluminum across the beam with a traversing screw and recording the detector output as a function of the position of the block. Before the block entered the beam there was no change in the detector output. The detector output decreased as the leading edge of the block crossed the beam. After the block completely blocked the beam the detector output no longer decreased. The local gamma beam strength was assumed to be proportional to the derivative of detector strength as a function of lateral position. The measured power profile was roughly Gaussian. The diameter of the gamma beam where the intensity was equal to 13.5% ($1/e^2$) of the maximum was 11 ± 1 mm.

In the second shakedown test the transient response of the gamma densitometer system was tested using a rotating polycarbonate disk with a diameter of 300 mm. The disk has seven wedge shaped sections having thicknesses of 0, 12.7, 25.4, 38.1, 50.8, 63.5 and 76.2 mm. The disk was placed in the gamma beam and rotated. The gamma densitometer accurately captured the transitions in thickness with the frequency response of the 60 Hz filter.

Following the shakedown tests, measurements were made of two-phase, air-water flows in the ribbed annulus. Tests were run for water flows ranging from 7.4 to 118 L/min and standpipe levels of 0.11 and 1.40 m of water with respect to the bottom of the annulus (Figure 1). The top of the rig was at atmospheric pressure. For most of the runs the gamma densitometer beam was positioned to pass through two opposite ribs. For some tests the gamma densitometer platform was rotated to measure local void fraction at other locations.

The procedure for the experiments was as follows:

1) The gamma densitometer output was logged with the annulus dry and again with it full of water.

2) A water flow was set and the pressure at the exit of the test section was set by means of a level in a standpipe. Air was entrained by the falling water and created a void fraction. Once steady state was achieved, pressure readings, entrained air flow and output of the gamma densitometer detector were recorded.

3) The length-average void fraction was measured by simultaneously inflating the bladder valves, which trapped the air and water mixture. The water was drained off and weighed. The mass of water that completely filled the space between the bladder valves had been weighed previously. Length-average void fraction was computed as one minus the quantity the mass of water collected under two-phase conditions divided by the mass of water that completely filled the space.

4) The gamma densitometer output was logged with the annulus dry and again with it full of water. It was necessary to repeatedly record the full and dry readings because the densitometer output drifted during the course of the day.

Data Reduction

The rate at which gamma photons pass through a material is given by the following equation;

$$I = I_0 e^{-\mu x} \tag{1}$$

where I_0 is the rate of photons entering the material, μ is the linear attenuation coefficient for the material and gamma wavelength under consideration and x is the thickness of the material or the path length through the material. The detector has an output voltage proportional to the rate at which photons enter it. Therefore, equation 1 can be written in terms of the detector voltage

$$V = V_0 e^{-\mu x} \tag{2}$$

where V_0 is the detector voltage with none of the material in the beam. The linear attenuation coefficient for cesium-137 gamma photons passing through water near room temperature is about 0.0091 per mm. The linear attenuation coefficient for air is about three orders of magnitude less. Therefore, absorption by air usually can be ignored. It is not necessary to know the linear attenuation coefficient for water if the detector output is measured with the flow channel both dry and full of liquid. Assume that B is the path length through liquid when the flow channel is full of liquid.

$$V_B = V_0 e^{-\mu B} \tag{3}$$

Solving equation 3 for the linear attenuation coefficient gives

$$\mu = \frac{1}{B} \ln \frac{V_0}{V_B} \tag{4}$$

Substituting equation 4 in equation 2 gives

$$\frac{V_0}{V} = \exp\left[\frac{x}{B} \ln \frac{V_0}{V_B}\right] \tag{5}$$

Recognizing that the fraction of the total path length that contains water (x/B) is equal to one minus the void fraction and rearranging equation 5 gives the equation for void fraction.

$$1-\alpha=\frac{\ln\frac{V_0}{V}}{\ln\frac{V_0}{V_B}} \qquad (6)$$

The terms V_0 and V_B were measured before and after each run with an air-water mixture. Linear interpolation was used to determine the values of V_0 and V_B at the time that the two-phase measurement was made. Those values as well as the instantaneous values of the densitometer output during the two-phase run were inserted in equation 6 to compute the instantaneous void fraction for each sample. Then a time averaged void fraction was computed.

Prediction of Void Fraction

Flach [14] assembled a set of equations that can be used to estimate either length-average void fraction or azimuthal-average void fraction at a particular axial location in a vertical channel. The mixture momentum balance is

$$\frac{dP}{dz}=[\alpha\rho_g+(1-\alpha)\rho_f]g-\frac{1}{2}\frac{f}{d_h}\rho_f\,|u_f|\,u_f \qquad (7)$$

Equation 7 assumes that the length vector, z, is in the downward direction of the flow, that accelerational effects are negligible and that the flow is steady. For the present data the Reynolds numbers were greater than 4000 and the appropriate equation for friction factor is

$$f=\left[1.14-2\log_{10}\left(\frac{\varepsilon}{D_h K_h}+\frac{21.25}{Re^{0.9}}\right)\right]^{-2} \qquad (8)$$

The phasic Reynolds number is

$$Re=\frac{\rho_f\,|u_f|\,D_h K_h}{\mu_f} \qquad (9)$$

The phasic and superficial liquid velocities are related.

$$u_f=\frac{j_f}{1-\alpha} \qquad (10)$$

For this geometry Flach gave the value of the hydraulic diameter correction factor, K_h, as 0.726.

The roughness, ε, was estimated from measurements of similar extruded tubes to be 2 μm. Void fraction estimates using the Flach prediction of void fraction, equations 7 through 10, will be presented along with the experimental results.

Experimental Measurement Uncertainties

The uncertainty in time averaged local void fraction, resulting primarily from instrument drift, was 0.04. The total uncertainty for the length-average void fraction is ± 0.014. The pressure gage calibrations were spot checked approximately once every two hours during testing. The resulting uncertainty was 0.14 kPa. The uncertainty for water flows less than 30 L/min was ±0.3 L/min. The uncertainty for higher flows was ± 3.9% of the reading. The uncertainty for each of the three air flow meters was ± 2.0 L/min.

Experimental Results

Measurements and predictions of length-average void fractions are plotted in Figure 3 as a function of water flow for standpipe levels of 0.11 and 1.40 m. Void fraction decreases monotonically with increasing flow. For the low standpipe level the extrapolated intercept on the void axis is almost one and for the high standpipe level the intercept is about 0.6. The reason for the second intercept is that even with no flow a column of water stands 1.27 m above the bladder valve or 32% of its length. Void fraction predictions agree well with measurements. One standard deviation for the difference between predicted and measured void fractions is 0.025.

Void fraction at the rib is plotted in Figure 4 and is less than length-average void fraction. Rib void fractions are somewhat lower for the higher standpipe level, which is consistent with the lower air flows at that standpipe level. It was necessary to compare the local void fraction, $\alpha(\theta, z=1.5\ m)$ with the azimuthal-average void fraction at the elevation of the local measurement, $\bar{\alpha}(z=1.5\ m)$. The bladder valve measurement gave the length-average void fraction, α_L. The azimuthal-average void fraction may be somewhat different than the length-average void fraction. The following procedure was used to compute a best estimate of the azimuthal-average void fraction at the gamma beam. The computation is based on the assumption that the difference between the true azimuthal-average void fraction and the measured length-average void fraction is equal to the difference between the predicted azimuthal-average void fraction and the predicted length-average void fraction. The preceding statement was placed in equation form and rearranged and the descriptor "best estimate" was substituted for "true".

$$\bar{\alpha}(z=1.5\ m)_{be} = \alpha_{L,meas} + \bar{\alpha}(z=1.5\ m)_{pred} - \alpha_{L,pred} \qquad (11)$$

The last term in equation 11 was evaluated for the measured pressure gradient over the length of

the annulus. The length-average pressure gradient was then input to the prediction of void fraction to calculate the length-average void fraction, $\alpha_{L,pred}$. The next to last term in equation 11 was evaluated for each run by first fitting the pressure data at five elevations in the annulus as a function of elevation with a quadratic. The quadratic was differentiated and evaluated at z equal to 1.5 m to determine the local pressure gradient at the elevation of the gamma densitometer. Then the local pressure gradient was input to the prediction of void fraction to calculate a predicted azimuthal-average void fraction, $\bar{\alpha}(z=1.5\ m)_{pred}$.

Figure 5 is a plot of void fraction at the rib versus best-estimate azimuthal-average void fraction. The data were fit by passing a line through the origin that minimized the sum of the squares of the differences between the line and the data. The result is

$$\alpha(\theta=0, z=1.5\ m)_{be} = 0.435\ \bar{\alpha}(z=1.5\ m)_{be} \qquad (12)$$

One standard deviation for data scatter around this line is 0.05.

The normalized azimuthal distribution of local void fraction for a standpipe level of 0.11 m and flows of 14.8 and 51.8 L/min is shown in Figure 6. Normalization was performed using equation 13 because the length-average void fraction varied ±2% for nominally identical conditions. The most likely reason for the variation was that the water flow or pressure boundary conditions varied somewhat from run to run.

$$\alpha_{norm,i}(\theta) = \alpha_i(\theta)\ \frac{\bar{\alpha}(z=5)_{pred,av}}{\bar{\alpha}(z=5)_{pred,i}} \qquad (13)$$

The terms $\bar{\alpha}(z=1.5\ m)_{pred,i}$ and $\bar{\alpha}(z=1.5\ m)_{pred,av}$ are the azimuthal-average void fraction for the *i*th run and the average of the azimuthal-average void fractions for all of the runs at the same hydraulic conditions. The term $\alpha_i(\theta)$ is the local measured void fraction for the *i*th run. The average of the azimuthal-average void fractions are also plotted. The data points at an angle of 15° were lost. However, the void fraction should be symmetrical so that the void fraction at 15° would be equal to the void fraction at 75°. The distributions are flat except at the rib where the local void fraction is significantly less. The local void fractions at the four non-rib positions are nearly the same as the average of the azimuthal-average void fractions which implies that only a small region near the rib has a reduced void fraction. The spatial discrimination of the gamma densitometer is limited by the diameter of the gamma beam. The beam width of 11 mm is equivalent to an angle of 12° at the average radius of the annulus or ±6° around the nominal

angle.

A commonly used relationship between air flow, water flow and void fraction is the drift flux equation [15].

$$\frac{j_g}{\alpha} = C_0 (j_g + j_f) + u_{jg} \qquad (14)$$

The terms C_0 and u_{jg} are the distribution parameter and the drift velocity. The terms C_0 and u_{jg} were determined using a least squares regression in which each point was weighted by the inverse of its uncertainty. The resulting values of C_0 and u_{jg} are 1.295 and 0.47 mps, respectively. Zuber and Findlay found that C_0 ranged from 1.2 to 1.6 and u_{jg} ranged from 0.27 to 0.49 mps for various air-water experiments in pipes. Clark and Flemmer [16] found that C_0 and u_{jg} were equal to 1.16 and 0.24 mps for air and water in a 51.6 mm pipe. The current value of C_0 is consistent with previous data whereas the current value of u_{jg} is at the high end of previous data. A possible reason for that is that the term u_{jg} is approximately equal to bubble rise velocity so when a bubble rises in a pipe it tends to move with an erratic lateral component to its motion which consumes additional energy. When a bubble rises in a ribbed annulus the ribs constrain the bubble laterally; however, the ribs do not seal and water can flow out of the annulus ahead of the bubble and back in behind it.

Conclusions

° Local void fractions measured with the gamma densitometer at locations away from the ribs were nearly equal (±0.03) to azimuthal-average void fractions.

° The best estimate for the void fraction at the rib is 44% of the azimuthal-average void fraction.

° Changing the pressure boundary at the bottom of the annulus does not make any obvious difference in the second conclusion.

Nomenclature

B	path length of gamma beam through liquid when flow channel is full
C_0	distribution parameter
f	friction factor
g	acceleration of gravity

I	photon rate
j_f	superficial velocity of liquid
j_g	superficial velocity of gas
u_{jg}	drift velocity
P	pressure
V	voltage
x	path length of gamma beam through liquid when flow channel is less than full
z	vertical coordinate
α	void fraction
μ	linear attenuation coefficient
ρ	density
θ	azimuthal coordinate

subscripts

be	best estimate
f	frictional or fluid
g	gas
L	full length of annulus
0	with no water in the gamma beam

References

1. Whatley, V., "Measurements of Void Fractions and Pressure Profiles for Downward Flowing Air-Water Mixtures in Single Test Annulus," WSRC-TR-90-328, 1990.

2. Flach, G. P., "WSRC-TR-90-328 Errata and Corrections," WSRC-TR-91-466, September, 1991.

3. Lahey, R. T., "Phase Distribution and Separation Phenomena in Two-Phase Flow," *Modern Developments in Boiling Heat Transfer and Two-Phase Flow*, short course conducted at Rensselaer Polytechnic Institute, June 25-29, 1990.

4. Oshinowo, Toks, and M. E. Charles, "Vertical Two-Phase Flow, Part I. Flow Pattern Correlations," *Canadian J. of Chemical Engineering*, vol. 52, pp. 25-35, 1974.

5. Herringe, R. A. and M. R. Davis, "Structural Development of Gas-Liquid Mixture Flows," *J. Fluid Mech.*, vol. 73, pp. 97-123, 1976.

6. Valukina, N. V., B. K. Koz'menko and O. N. Kashinskii, "Characteristics of a Flow of Monodisperse Gas-Liquid Mixture in a Vertical Tube," English translation, *Inzhenerno-Fizicheskii Zhurnal*, vol. 36, #4, pp. 695-699, April, 1979.

7. Zun, I, "The Traverse Migration of Bubbles Influenced by Walls in Vertical Bubbly Flow," *Int. J. Multiphase Flow*, Vol. 6, pp. 583-585, 1980.

8. Nakoryakov, V. E., O. N. Kashinsky, A. P. Burdukov and V. P. Odnoral, "Local Characteristics of Upward Gas-Liquid Flows," *Int. J. Multiphase Flows*, vol. 7, pp. 63-81, 1981.

9. Sadatomi, M. and Y. Sato, "Two-Phase Flow in Vertical Noncircular Channels," *Int. J. Multiphase Flow*, vol. 8, pp. 641-655, 1982.

10. Gorelik, R. S., O. N. Kashinskii and V. E. Nakoryakov, "Study of a Downward Bubbly Flow in a Vertical Pipe," English translation, *Zhurnal Prikladnoi Mekhaniki i Tekhnicheskoi Fiziki*, #1, pp. 69-73, Jan.-Feb, 1987.

11. Wang, S. K., S. J. Lee, O. C. Jones and R. T. Lahey, "3-D Turbulence Structure and Phase Distribution Measurements in Bubbly Two-Phase Flows," *Int. J. Multiphase Flow*, vol. 13, pp. 327-343, 1987.

12. Bentley, Charles and Art Ruggles, "Phase Distribution Measurements in Narrow Rectangular Channels Using Image Processing Techniques," FED-Vol. 125, *Experimental Techniques in Multiphase Flows*, ASME, 1991.

13. Steimke, J. L., "Azimuthal Variation of Void Fraction in a Ribbed Annulus", WSCR-TR-91-

661, 1992.

14. Flach, G. P., "Void Fraction Estimation Program Available," NES-CDG-910062, April 1991.

15. Zuber, N. and J. Findlay, "Average Volumetric Concentration in Two-Phase Flow Systems," *J. Heat Transfer*, vol. 87, p. 453-468, 1965.

16. Clark, N. N. and R. L. C. Flemmer, "On Vertical Downward Two-Phase Flow," *Chemical Engineering Science*, vol. 39, pp. 170-173, 1984.

Figure 1
Void Fraction Rig

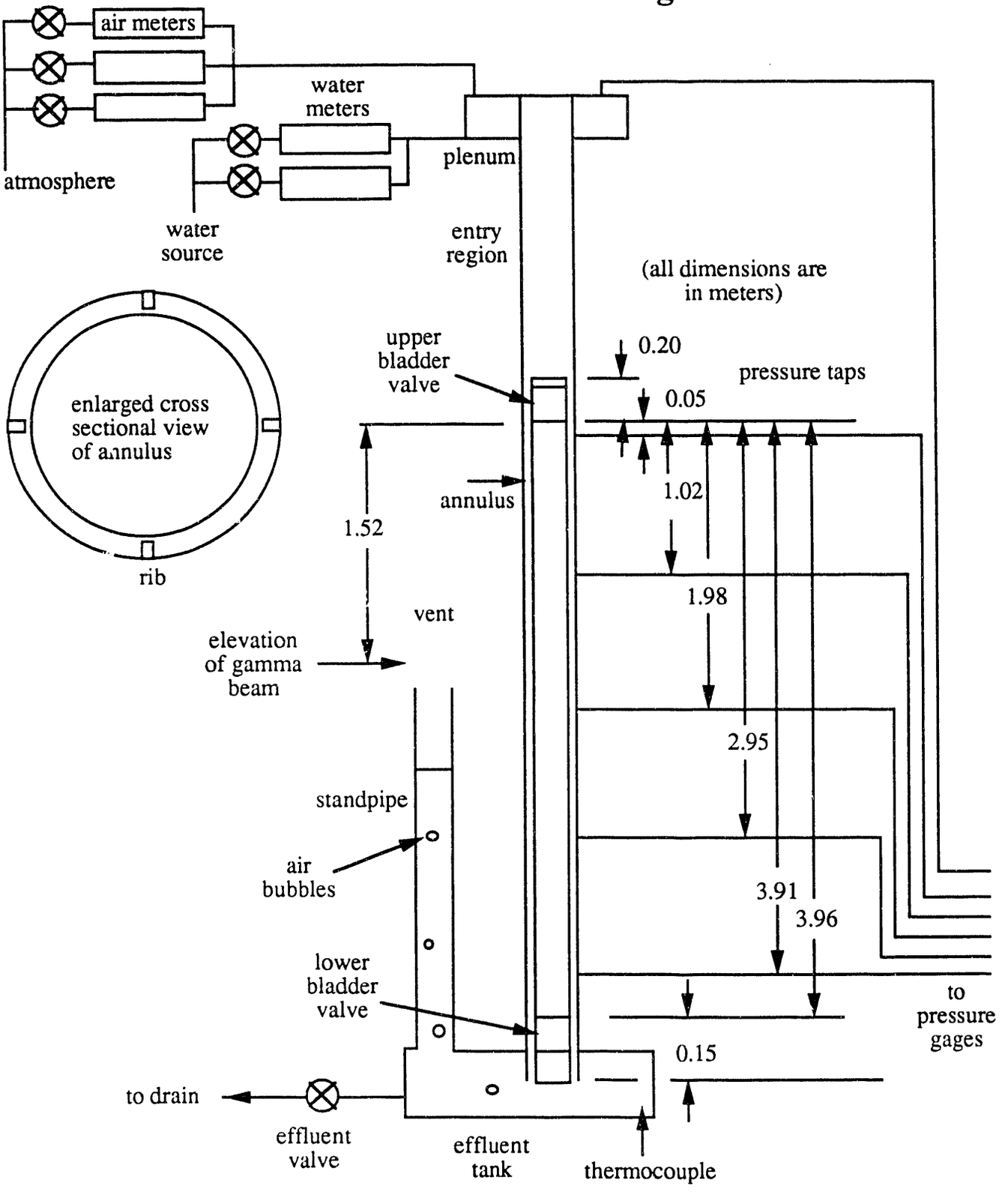

Figure 2
Alignment of Gamma Beam on Ribbed Annulus

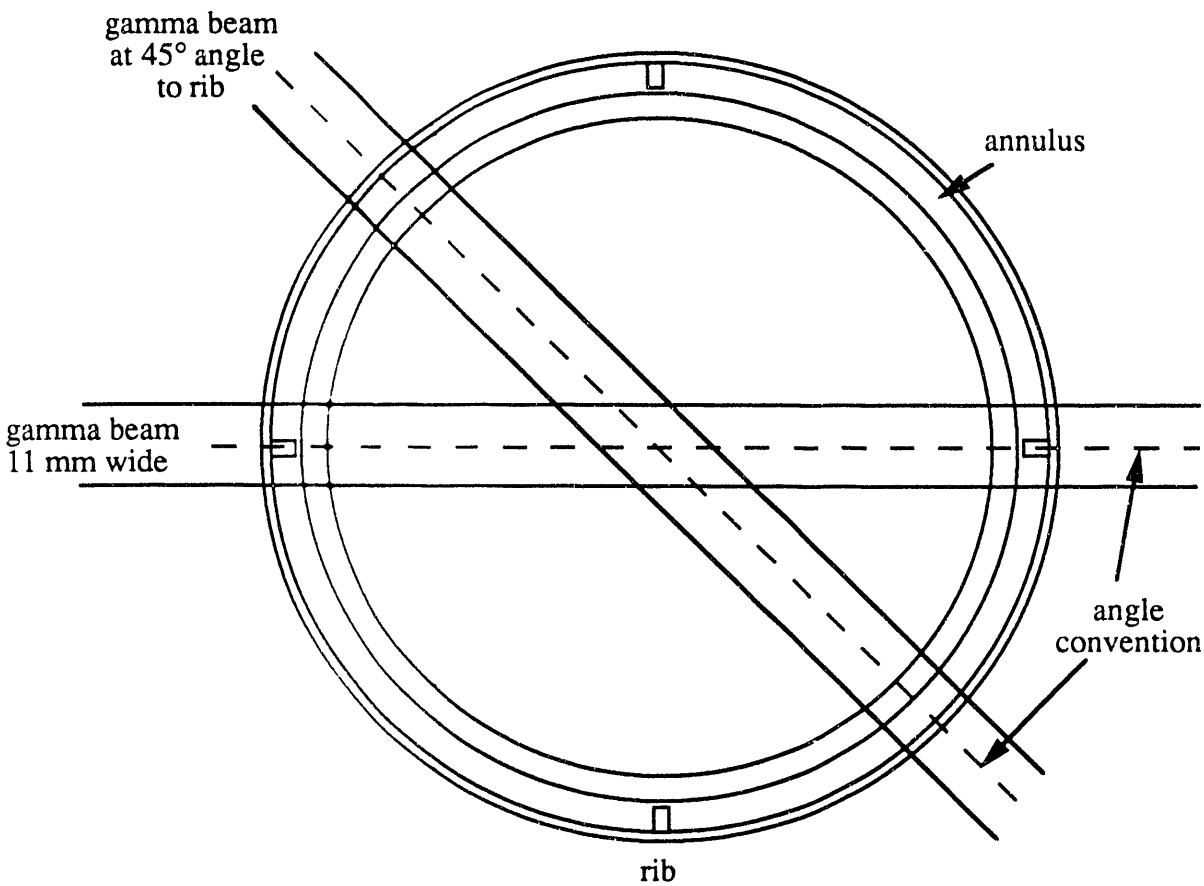

Figure 3
Length Average Void Fraction

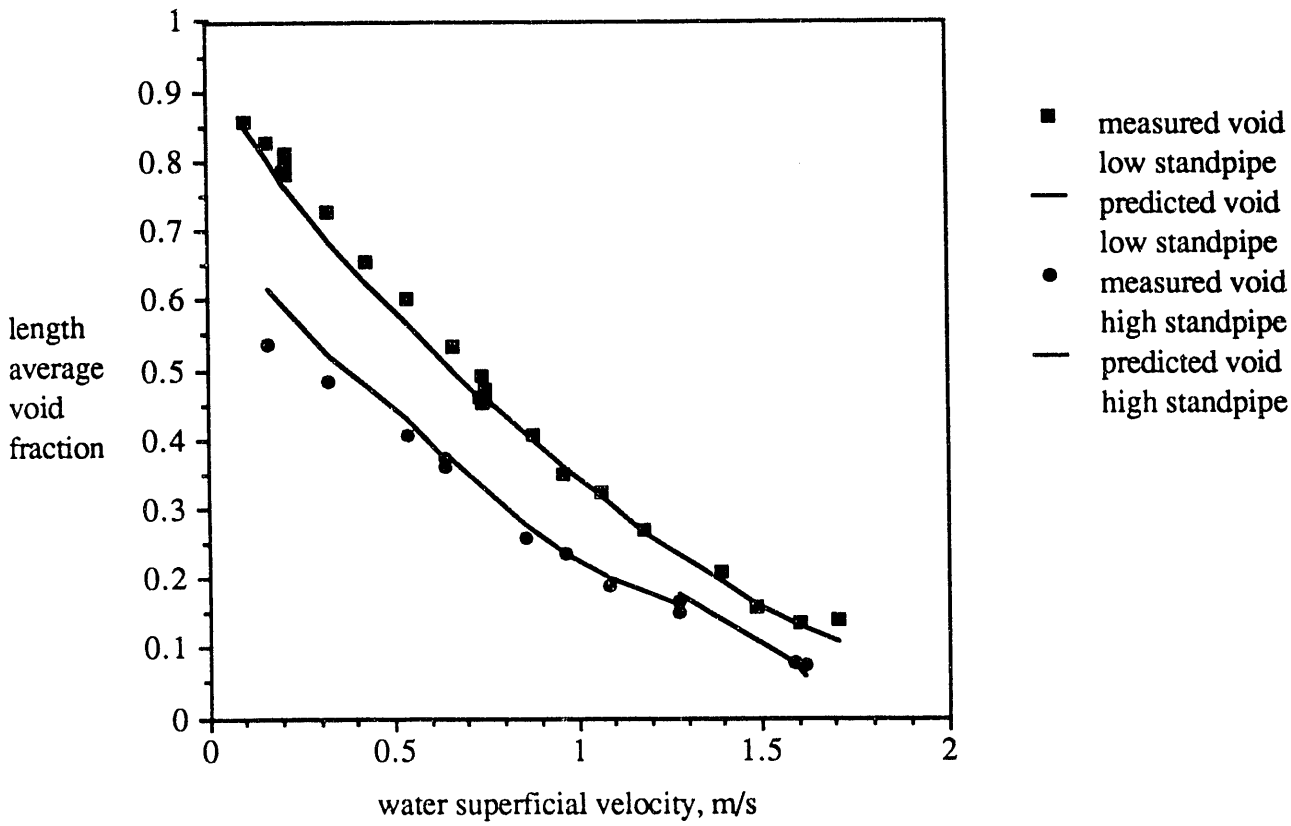

Figure 4
Local Void Fraction at Rib

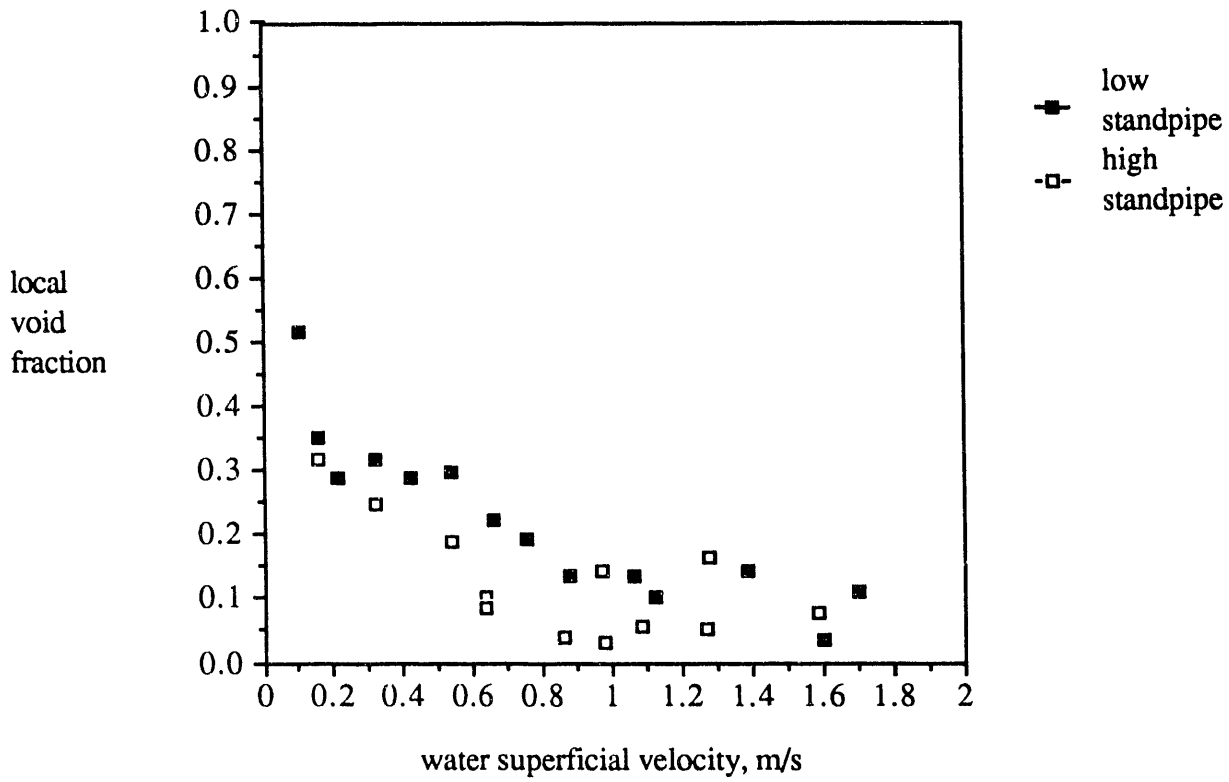

Figure 5
Rib Void as Function of Azimuthal Average Void Fraction at Gamma Densitometer

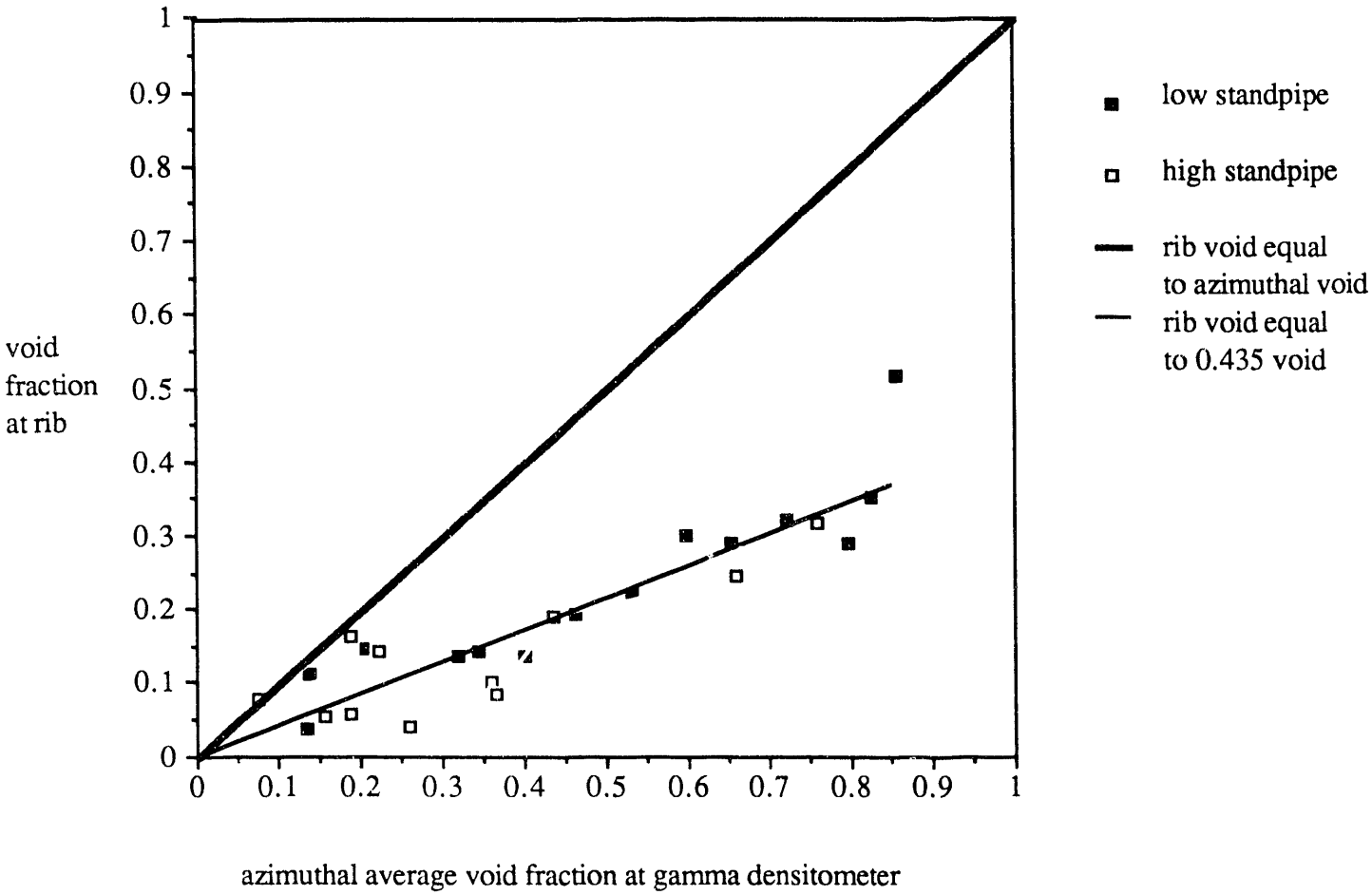

Figure 6
Azimuthal Distribution of Local Void Fraction

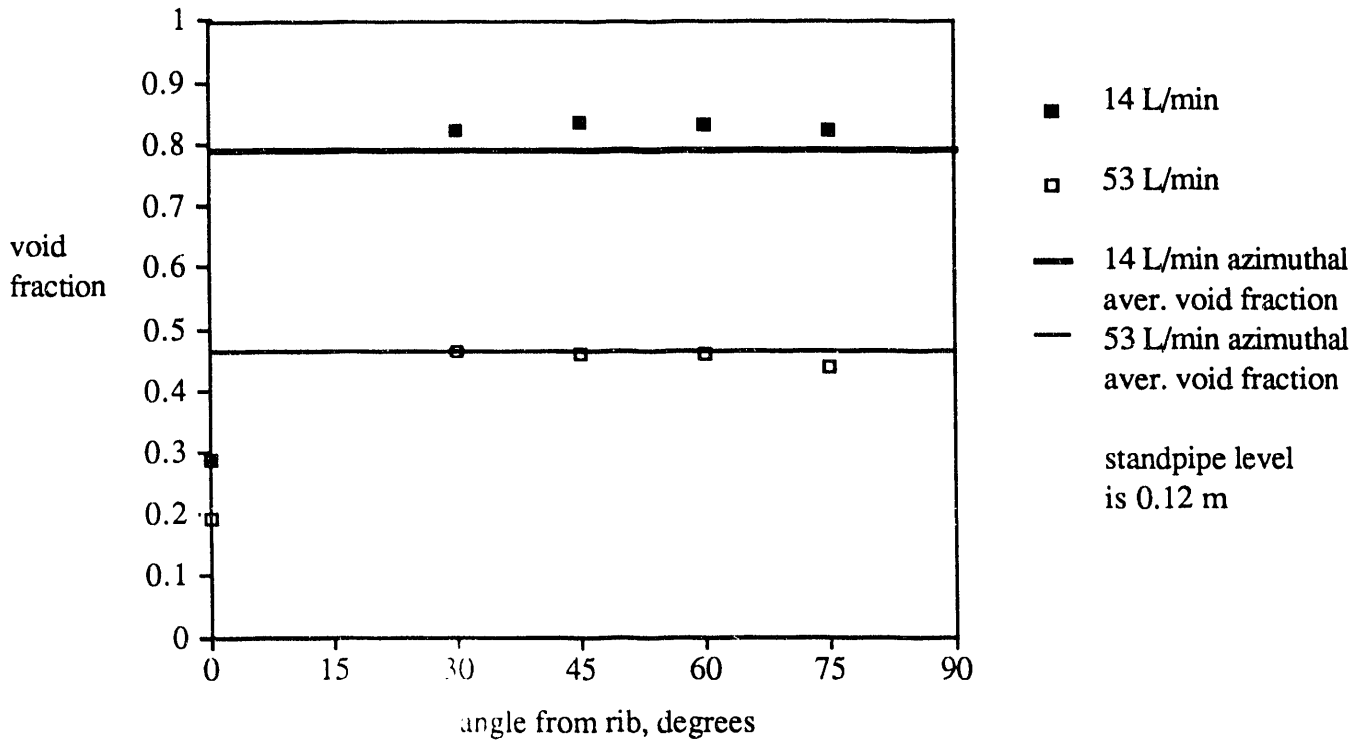

END

DATE
FILMED
7/12/93